Plant Physiology Preview. Published on March 18, 2015, as DOI:10.1104/pp.114.256271

Running head: high resolution cavitation- and frost-fatigue

Corresponding author:
Melvin T. Tyree
College of Forestry, Northwest A&F University, Yangling, Shaanxi 712100, China
E-mail: mel.tyree@cantab.net
Telephone: +86 029 87080363

Research area:
Ecophysiology and Sustainability

Investigations concerning cavitation- and frost-fatigue in clonal *Populus* 84K using 'high resolution' cavitron measurements[1]

Feng Feng, Fei Ding, Melvin T. Tyree*

College of Forestry, Northwest A&F University, Yangling, Shaanxi 712100, China

*Author for correspondence mel.tyree@cantab.net

Summary:

Frost and drought induced ‘fatigue’ in *Populus* stems, which damaged vessels making them more vulnerable to embolism in future; evidence supports a common mechanism causing both types of fatigue.

Footnotes

[1] This study was supported by the grants of “thousand talent program” to M.T.T.

* Corresponding author; email mel.tyree@cantab.net

Abstract

Both drought and freezing-thawing of stems induce a loss of hydraulic conductivity (PLC, percent loss of conductivity) in woody plants. Drought induced PLC is often accompanied by physical damage to pit membranes causing a shift in vulnerability curves (cavitation-fatigue). Hence if cavitated stems are flushed to remove embolisms, the next vulnerability curve is different (shifted to lower tensions). The *Populus* clone (84K *Populus alba*×*Populus glandulosa*) has small vessels that should be immune from frost-induced PLC, but results demonstrated that freezing-thawing in combination with tension synergistically increased PLC. Christensen-Dalsgaard & Tyree were the first to define 'frost-fatigue' which is similar to cavitation-fatigue but induced by freezing. Frost-fatigue caused a transition from a single- to a dual-Weibull curve but drought-fatigued stems had single-Weibull curves shifted to lower tensions. Studying the combined impact of tension plus freezing on fatigue provided evidence that the mechanism of frost-fatigue may be due to extra water tension induced by freezing or thawing while spinning stems in a centrifuge rather than direct ice-damage. A hypothesis is advanced that tension is enhanced as ice crystals grow or melt during the freeze or thaw event, respectively, causing a nearly identical fatigue event as induced by drought.

INTRODUCTION

Water transport in xylem conduits of trees occurs while water is under tension (= negative pressure) (Tyree and Zimmermann, 2002). The xylem water-transport system is vulnerable to cavitation and embolism, because tensile water is meta-stable so if a gas bubble appears in a conduit it will rapidly expand to fill the conduit whenever the fluid tension is ≥ 0.1 MPa, where a tension of 0.1 MPa is equivalent to vacuum-pressure. A cavitation event occurs whenever a tensile water-column breaks which results in a water-vapor-filled void. Because of Henry's law of gas solubility in water, this vapor-void will eventually equilibrate with air at atmospheric pressure at which point the conduit is fully embolized (Tyree and Zimmermann, 2002). Embolism has been identified as a limiting factor of primary production (Hubbard et al., 2001). As a result, tree growth and fitness are probably negatively impacted temporarily or seriously limited permanently if embolism is extensive (Christensen-Dalsgaard and Tyree, 2013).

The two main factors causing cavitation and embolism are drought and frost (Mayr et al., 2003; Christensen-Dalsgaard and Tyree, 2013). Drought-induced cavitation is caused by the high xylem tension attributed to water stress. The high tension in the sap forces air bubbles into functional conduits from neighboring embolized ones through shared pit membranes (Jarbeau et al., 1995; Sperry et al., 1996; Hacke et al., 2001; Stiller and Sperry, 2002; Christman et al., 2012) according to "air seeding" mechanism (Sperry and Tyree, 1988; Cochard et al., 1992). Hence, the continuity of water flow is disrupted due to cavitation. Frost-induced cavitation, on the other hand, occurs when dissolved gases in the sap freeze out and create bubbles during ice formation because air is not soluble in ice (Mayr et al., 2003; Christensen-Dalsgaard and Tyree, 2013, 2014) but remains entrapped between ice crystals. Once the sap melts and tension is re-generated, the entrapped bubbles may expand to embolize the conduits instead of dissolving (Pittermann and Sperry, 2006). Current thinking is that freezing-induced embolism occurs when the tension exceeds a critical value determined by the surface tension of the bubbles, which mainly depends on the xylem water potential and the bubble radius (Yang and Tyree, 1992; Tyree et al., 1994; Hacke and Sperry, 2001). Larger bubbles may form in conduits with a larger diameter, so species with larger conduits are more vulnerable to frost-induced embolism (Langan et al., 1997; Davis et al., 1999; Pittermann and Sperry, 2006). Furthermore, enhanced loss of hydraulic conductivity of trees may occur when stems are subjected to a combination of frost-drought causing low xylem water potential (Mayr et al., 2003; Willson and Jackson, 2006) and repeated freeze-thaw cycles (Sperry and Sullivan, 1992; Cox and Zhu, 2003; Mayr et al., 2003). However, even trees with small conduits are found to suffer severe embolism in winter (Sperry et al., 1988; Ameglio et al., 2002) due mostly to freeze-drying of stems.

Resilient species are those which suffer no significantly different cavitation resistance before and after a cavitation-refilling cycle (Hacke et al., 2001; Christensen-Dalsgaard and Tyree, 2013). In contrast, species that are weakened by cavitation or frost are said to suffer cavitation-fatigue or frost-fatigue. Cavitation and frost-fatigue is quantified by how much the vulnerability curve is shifted before versus after a fatigue-inducing event, and it is typically reported as a shift in P_{50}. The P_{50} is either the pressure (negative value) or tension (positive value) that produces 50 % loss of hydraulic conductivity (K_h). In the rest of this paper we will use T_{50} to indicate the tension at 50 % loss of conductivity or T_x to indicate the tension that induces x % loss of conductivity. Vulnerability curves (VCs) are usually measured by a centrifuge technique (Alder et al., 1997; Cochard et al., 2005), but most people measure just 5 or 6 points to determine a VC. "High resolution" VC curves with 9 to 27 points per curve can be collected quickly using the Cochard rotor. Recent studies have successfully used high resolution VC to characterize the detailed shape of VCs revealing dual-Weibull curves, e.g., r- and s- shaped or dual s-shaped curves (Cai et al., 2014; Wang et al., 2014a), because a complex shape to a VC cannot be identified with just a few points. Furthermore, we used a centrifuge to induce tension while simultaneously freezing in order to study the combined impact of tension and freezing-thawing on frost-fatigue and freeze-thaw-induced embolism.

In this paper, we intend to investigate whether drought and freeze-thaw cycles could have an effect on the cavitation resistance in terminal shoots from adult trees of 84K poplar (*Populus alba* × *Populus glandulosa*), with high resolution analysis of VCs and artificial freeze-thaw simulation technique. *Populus* are known to be water-demanding, drought-sensitive species with T_{50} ranging from 1.07 to 2.5 MPa (Fichot et al., 2014) and vulnerable to winter damage (Feng et al., 2010). Amongst poplars, 84K poplar is known by foresters to be relatively resistant to water stress, low temperature, diseases and insects (Zhou et al., 2007). As the main afforestation species in Shaanxi, Gansu and Qinghai Province, 84K is of great ecological importance.

RESULTS

Cavitation-fatigue

Vulnerability curves of 84K stems were measured 4 times; the first VC was measured in flushed, native material and the other 3 VCs were obtained on the same stem segments after exposure to 3 cycles of flushing with 0.1 M KCl and 0.01 M $CaCl_2$ solutions followed by VC measurements. All VCs were s-shaped and fit Weibull curves with an average route mean square error (RMS_{error}) of 2.31 %; see Fig. S1A for typical curves. The recovery of K_h after each flush cycle averaged about 99.48 % for all experiments (Table I). The mean values ± SE of tension (T_x) at 10 % increments of PLC are shown in Table II together with results of a significance test between KCl

and $CaCl_2$ treatments. There was no significant difference between T_x values for KCl and $CaCl_2$ perfusions except between the 2nd and 3rd VC where $CaCl_2$ perfusion made the stems significantly more vulnerable from x = 10 to 50 PLC.

The shift of vulnerability curves to the left in Fig. 1 indicated a loss of cavitation resistance (cavitation-fatigue), but a shift to the right indicated a gain of cavitation resistance (recovery from cavitation-fatigue). The significance of the shift in VCs was calculated two ways: shifts of mean VCs and shift between stems (see Eq. 3 in Methods). The significance tests based on shifts of means is shown in Table III. There were significant difference between the 1st versus 2nd, 1st versus 3rd, and the 1st versus 4th VC for both KCl and $CaCl_2$ flushed stems and between the 2nd and 4th VCs for KCl flushed stems based on the means in Table II.

The significance test for shifts in the mean values of T_x were confounded by the population variability of VCs between individual stems. A stronger test of the shift in T_x values is obtained by using Eq. 3B to compute the means shift of all individual branches and testing if the shift is significantly different from zero. The shifts can be computed as absolute cavitation-fatigue shifts (aCF_x) or relative cavitation-fatigue shifts (rCF_x) as defined in Eq. 3 and these are shown as plots in Fig. 2 and 3. Fig. 2 and 3 demonstrated that there was a positive increase in cavitation-fatigue (positive aCF_x or rCF_x) between the 1st and 2nd VC. But there were small but significant improvements (negative aCF_x or rCF_x) for most other cycles. Negative values of aCF_x or rCF_x indicate the resistance to cavitation improved. Stems flushed by KCl solutions recovered more than stems flushed with $CaCl_2$ solutions (Fig. 2&3).

Frost-fatigue and frost-induced PLC

The vulnerability curves of 84K poplar were sigmoid curves in all experiments even after cavitation-fatigue had occurred (Fig. 1 and S1A). In contrast, our freeze-thaw treatments caused significant change in the shape of the VCs measured after flushing. They changed from single to dual s-shaped Weibull curves (Fig. 4 and S1B, Eq. 2B). Freeze-thaw cycles were conducted on flushed stems at 4 different tensions 0.088, 0.5, 1.0 and 1.5 MPa while the stems were spinning in a cavitron, and the mean flushed conductivity after the freeze-thaw event was ≥95 % of the original (Table I). The highest two tensions were enough to cause some cavitation-fatigue in the absence of freezing but there was a synergy between the freeze-thaw event and cavitation-fatigue causing a higher loss of maximum conductivity (Fig. 5) than expected from cavitation-fatigue alone. At the lowest three tensions the frost-fatigued curves were not significantly different and involved a shift in the 10 to 15 % of most vulnerable vessels (Fig. 4). However, a freeze-thaw cycle at tension = 1.5 MPa caused a significant increase in frost-fatigue.

The mean vessel diameter of 84K poplar was 28.70±0.11 μm (N = 4307) and hence should not be big enough to induce loss of conductivity during a freeze-thaw event (Hacke and Sperry,

2001) and this fact is confirmed in the near-zero tension value shown in Fig. 5; nevertheless frost-fatigue occurred even at the lowest tension (Fig. 4). However increased tension caused a reduction in maximum K_h (Fig. 5) wherein the loss of K_h exceeded that due to tension-induced cavitation without freezing. This suggests that the freeze-thaw event caused an increase in tension (double arrows in Fig. 5) during either the freezing or during thawing or both as explained in the Discussion.

Frost-fatigue VCs looked very different from cavitation-fatigue VCs, because the former transformed an s-shaped curve into a dual s-shaped curve whereas cavitation-fatigue shifted the entire s-shaped curve to the left in Fig. 1 but it remained a simple s-curve. We postulated that frost-fatigue might damage only the most vulnerable vessels, hence the nature of the damage might be duplicated by cavitation-fatigue in only the lower half of the VC. To test this notion we measured vulnerability curves of stems only to the 50 PLC value (Fig. 6, solid line), flushed the stem then measured the VC again (Fig. 6, dashed curve). This procedure produced a dual Weibull strikingly similar to our frost-fatigue curve (Fig. 4, dotted line).

Field observations of frost-fatigue

Vulnerability curves measured in four consecutive phenological phases were plotted in Fig. 7A. The VCs were not significantly different from each other no matter how many freeze-thaw cycles occurred during the winter (Table IV). The frequency of frost events in the winter of this study can be deduced from the maximum and minimum temperatures shown in Fig. 7B, but the stems might not have frozen every time the air temperature fell below 0 ^{o}C because of super-cooling. However, once leaves were fully expanded values of T_{60} to T_{90} declined perhaps because of growth of new vessels in spring. The frost-fatigue in early winter suggested that some of the early winter freezing events were enough to cause some frost-fatigue that persisted into the spring. Comparison of Fig. 7A to Fig. 4 through 5 suggests that the first natural freezing events in trees might have been accompanied by an enhancement of xylem tensions of ≥ 0.5 MPa at the time of the freeze-thaw events. Frost-fatigue hydraulically damaged about 16 % of the most vulnerable vessels (Fig. 7A). These freeze-thaw events caused no significant shift in the T_{50} (see Table IV and II), hence the events reported in this paper would not have been observed in previous studies that reported only the impact of frost damage on T_{50} (Christensen-Dalsgaard and Tyree, 2013). High resolution vulnerability curves are needed to document the cause of dual-s Weibull curves. At the beginning of our research on 84K poplar, dual-s Weibull curves were observed in June and July. By August the 84K poplar shoots grew enough for cavitron sized stem segments (0.274 m long by 6 mm diameter) to include only current year shoots. Hence, when cavitation-fatigue experiments began in August only s-shaped curves were observed (see Fig. 1). When the trees

flushed new leaves after winter, the vulnerability curves were still dual Weibull similar to those measured in the winter.

DISCUSSION

The present study revealed two different fatigue responses in 84K poplar: a strong drought-induced cavitation-fatigue and a weaker frost-induced fatigue. These will be discussed separately below.

Cavitation-fatigue: relative (rCF_x) and absolute (aCF_x)

Many prior studies have described cavitation fatigue, see Hacke et al. (2001) and papers cited therein. The unique findings of our study were: (1) That repeated cycles of cavitation and flushing do not cause additional damage, i.e., repeated cycles of cavitation and flushing did not increase the magnitude of fatigue (Fig. 1) rather our data showed significant partial recovery (Figs. 2 and 3). (2) That high resolution measurements of VCs revealed pattern of cavitation-fatigue in which the rCF_x was a linear function of the tension (T_x) causing the fatigue (Fig. 2A and 3A) wherein the most vulnerable vessels exhibit the most relative cavitation-fatigue. (3) That when minor recovery from cavitation-fatigue occurred after three cycles of cavitation and flushing, the biggest recovery occurred among the most vulnerable vessels. (4) That repeated cycles of flushing and cavitation showed that $CaCl_2$-flushed stems exhibited poorer recovery than KCl-flushed stems (see Fig. 2 and 3).

With regard to the last finding, we compared stems flushed with $CaCl_2$ versus KCl to investigate the possible role of Ca^{2+} in stabilizing cell walls and pit membranes (Cosgrove, 1997; van Ieperen and van Gelder, 2006). Cell walls are weak ion exchange resins containing mostly polyuronic acids that normally favor the accumulation of Ca^{2+} at the weak acid exchange sites. Repeated flushing with concentrated KCl would gradually eliminate nearly all Ca absorbed to the exchange sites. Ca^{+2} might serve as a bridge between weak acid polymers that might add to the stability of pit-membrane pores that seed cavitation. Our results conclusively show that washing out Ca^{2+} by flushing with 0.1 M K^+ enhanced rather than weakened cavitation resistance from which we might conclude that putative pit-membrane pores actually shrunk. In contrast, flushing with Ca^{2+} made no difference compared to K^+ and may actually retard recovery from cavitation-fatigue.

Trends of rCF_x versus T_x had slopes significantly different from zero. In other species of *Populus* the vulnerability to cavitation (measured by the b constant in the Weibull function) was linearly related with vessel diameter (Cai and Tyree, 2010). Hence it can be hypothesized that the larger vessels have more relative cavitation-fatigue (rCF_x). More research is needed to confirm this relationship. Values of rCF_x in other species are also worth documenting in the future.

In our study 'drought' was induced artificially in a centrifuge but it is generally assumed that soil-based drought events will have the same impact on cavitation-fatigue, although there are few examples proving that assumption with the notable exception of the well-documented case of sunflower (Stiller and Sperry, 2002). In the case of sunflower, potted plants were dehydrated by withholding water and the stem recovered from drought induced cavitation-fatigue within 4 days of re-watering, whereas the excised stems cavitated in a centrifuge showed weak or no recovery. Our study on 84K poplar also showed small but significant recovery from cavitation-fatigue. More comparisons between whole plants and excised shoots need to be done to understand the mechanism of recovery in whole plants. In a survey study of 7 species, Hacke et al. (2001) found that three species were 'resilient' and four species were not resilient. Among the four species in (Hacke et al., 2001) two were *Populus sp.* that exhibited cavitation-fatigue in agreement with our 84K-clone *Populus*. In contrast, Christensen-Dalsgaard and Tyree (2013) have reported the Walker-clone *Populus* to be resilient in terms of T_{50}.

Absolute Frost-fatigue (aFF_x) and Frost-Induced PLC

In contrast to cavitation-fatigue in which the pre- and post-fatigued stems were both s-shaped, frost-fatigue changed the VC from an s-shape to a dual s-shape. Most previous studies of frost-fatigue (Hacke and Sperry, 2001) have focused on increased PLC after a freeze-thaw event and frost-fatigue was measured as a shift of 4 to 5 point VCs of unfrozen versus frozen samples. Christensen-Dalsgaard and Tyree (2014) focused on shifts of $T_{25,}$ T_{50} and T_{90} from VCs with 6 to 7 points. Our study is unique in quantifying high resolution curves with > 20 points depending on the complexity of the curve. High resolution curves are needed to accurately resolve complex curve shapes.

From previous studies we would predict that 84K poplar would exhibit no PLC or frost-fatigue following a freeze-thaw cycle because vessel diameter of 84K poplar (28 μm) was below the critical diameter of 30 μm (Davis et al., 1999). Species with vessel-diameters 40 μm are typically 100 % embolized after a freeze-thaw event whereas species with vessels between 30 and 40 μm diameter are intermediate (Davis et al., 1999). Our results demonstrated that tension in combination with a freeze-thaw event caused more PLC than tension alone (see Fig. 5). Our study is the first to demonstrate that species with vessels < 30 μm diameter are impacted when frozen under tension, which caused increased PLC and frost-fatigue. It is not clear whether frost-induced embolism is always accompanied by frost-fatigue nor do we fully understand the mechanism of damage to pit membranes making them more vulnerable to cavitation after a freeze-thaw event.

Our results were consistent with the notion that a freeze-thaw event increased the centrifuge-induced "background" tension present in the stem segment during the experiment. Hence more research is justified to test the hypothesis that cavitation-fatigue and frost-fatigue might both be

manifestations of cavitation-fatigue. The idea that a common mechanism existed between frost- and cavitation-fatigue was confirmed by the cavitation-fatigue experiment in which the first VC was taken only to 50 % PLC, because when these stems were flushed the cavitation-fatigue that resulted was strikingly similar to the frost-fatigue VC (compare Figs. 6 to 4).

Comparing the results in Fig. 5 (dashed line minus solid line) one can conclude that the freeze-thaw cycle increased the tension by about 0.5 to 0.8 MPa (double headed arrows in Fig. 5). Since water expands to form ice as it freezes and contracts as it thaws one might presume the frost-fatigue occurred during the thaw. But this simple notion might be wrong, because when *Acer* and *Juglans* stems freeze the tension often occurred during the freeze and positive pressure occurred during the thaw. Readers should consult previous work on *Acer* for the detailed explanation for this notable behavior (Tyree, 1983; Johnson et al., 1987; Cirelli et al., 2008). Briefly, however, the development of tension is due to water migration into air-filled wood fiber cells to form ice (O'malley and Milburn, 1983; Milburn and O'malley, 1984) during the freeze event. The ice formation in the Milburn-O'Malley model is by vapor distillation from water in vessels to ice-crystals growing in air-filled spaces and the distillation process will induce tension in the liquid water. Our suggested interpretation of Fig. 5 is as follows: In flushed stems all wood fiber cells are filled with water so freezing induces no extra tension hence there can be no freezing induced PLC. But if the stems are put under tension before freezing then air-spaces are created in some fiber cells where ice can form causing freezing-induced tension by the Milburn-O'Malley model (Tyree 1983; Milburn and O'Malley 1984); the enhanced tension would then induce cavitation before the vessels are totally frozen. However, the parsimonious explanation is that bubbles entrapped in ice expand during the thaw while ice melts under tension. We reject the parsimonious interpretation because a tension of 0.5 MPa should be enough to induce 100 % embolism in all vessels because all vessels have air entrapped in ice. In contrast the Milburn-O'Malley model predicts that tension will increase as the amount of air space for ice formation increases and the volume of air-filled fibers might increase with tension. Future research may resolve these conflicting ideas.

An alternative explanation is that ice-crystal formation somehow damages pit membranes (Christensen-Dalsgaard and Tyree, 2014). For this to occur ice crystals have to grow faster on one side of pit membrane than the other. This is highly likely to occur if one side has water that can freeze but the other side has air, because as water expands 10 % to form ice the pit membrane could be pushed towards the embolized side causing tensile failure to the membrane. In contrast, if water and ice are present on both sides of the pit membrane the pressure of ice might oppose each other equally resulting in no damage. This idea about 'one-sided' ice growth cannot be tested

in 84K poplar, because embolizing 50 % of the vessels induced about the same amount of fatigue measured as a shift in vulnerability curve at the lower PLC-values as frost-fatigue.

Comparing Figs 1 and 6 reveals a shift of aCF_x (at x = 10 PLC) of about 1 MPa and this shift is the same as the frost-fatigue shift (aFF_x) at 10 PLC (Figs. 4 and 7). It could be argued that ice-induced damage to pit-membranes ought to be quite different from cavitation damage. During a cavitation event only one pore out of millions of pores connecting adjacent vessels needs to be plastically deformed to make a larger hole which makes the vessels more prone to cavitation in subsequent VCs (Fig. 1). Based on surface tension arguments (Tyree and Zimmermann, 2002), we can say that the diameter (D) of a pit membrane pore that induces cavitation should be = $cos(\theta)$ $4\gamma/\Delta P$, where ΔP is the pressure difference inducing cavitation across the pore and θ is the contact angle of the air/water interface at the pore surface and γ is the surface tension of the solution at the pit pore. Frost- or cavitation-fatigue (aFF_x or aCF_x, respectively) equals the shift in ΔP to ΔP_f, i.e., from a normal to fatigued pressure difference inducing cavitation. Hence $D_f = D\ \Delta P/\Delta P_f$. The shift of aCF_x at 10 PLC is ΔP= 1.5 to ΔP_f =0.5 MPa from which it follows that the most fatigued pore in the pit membrane is 3 times larger than the native pore (because $\Delta P/\Delta P_f$.=3). The magnitude of $aCF_x = aFF_x$ in our study (at x = 10 PLC), which is a remarkable coincidence. One might argue that if growth of ice-crystals is poking holes in pit membranes, the holes ought to occur in thousands of membrane connecting adjacent vessels and it seems unlikely that the shift aFF_x and aCF_x would be nearly identical. More experimental work might provide useful data to resolve the above speculations.

We think much more can be learned about cavitation- and frost-fatigue through high resolution measurement of vulnerability curves in a Cochard cavitron. At the time this study was completed we could achieve fits to single or dual Weibull curves with RMS_{error} of about 2 %. The RMS_{error} was primarily due to the error in estimation of K_h and K_{max} because PLC = 100(1 - K_h/K_{max}). Subsequent to the completion of this study we were able to increase the precision of measurements of K_h and K_{max} by a factor of 5 (Wang et al 2014b). The increase of precision was achieved by using a regression method to estimate hydraulic conductivity values and by using a centrifuge that can control temperature of the stem to ±0.04 ^oC. Temperature control is important because K_h is inversely proportional to 1/viscosity of water and the viscosity changes about 2.4 % $^oC^{-1}$. By using high resolution measurement (more points) and high precision measurements (more accurate K_h), future studies on cavitation- and frost-fatigue may reveal more about the mechanisms of damage and about the linkage, if any, between the two types of fatigue.

MATERIALS AND METHODS

Plant material

The study was carried out on the clonal *Populus* 84K (*Populus alba*×*Populus glandulosa*) growing near Northwest A&F University, Yangling, Shaanxi, China (34°15'N 108°4'E, Elev. 457 m). The sampling was conducted at intervals from August to April over a fall-winter-spring season in 2013-2014. All measurements were done on shoots that were not significantly water stressed before collection because no evidence of cavitation-fatigue was observed in the first VC after flush. Shoots 90- to 120- cm length were excised, because preliminary air-injection experiments indicated that maximum vessel length was < 50 cm and mean about 6 cm, hence the vessels are short enough relative to cavitron sample length to avoid 'open-vessel' artifacts reported by Wang et al. (2014a). The branches were enclosed in humidified black plastic bags after spaying leaves with water. Then they were transferred to the laboratory within 15 min and submerged in water for at least 30 min to release tension. While submerged, a 27.4-cm-long segment was cut from each branch using fresh razor blades. Leaves were removed when present. These segments were exposed either to four consecutive cycles of cavitation-refilling or to a freeze-thaw cycle in combination with tensile-water, imposed by spinning stems in a centrifuge. Additional experiments were done on the same species to compare lab results with field conditions throughout the winter and spring.

A vulnerability curve (VC) defines the relationship between percentage loss of hydraulic conductivity (PLC) and the tension (T), where T = minus the xylem pressure potential. We used the whole vulnerability curves to quantify "fatigue" over 9 equally spaced points on the y-axis of the VC (for simple s-shaped curves). The cavitron technique was used to measure vulnerability curves. Both cavitation and frost-fatigue were measured in terms of the shift of the vulnerability curve along the tension axis.

Flushing with particle 'free' water

Clean flushing water was essential to prevent plugging of pit membranes in the segments (27.4 cm long) because one objective was to carry out 4 repeated cycles of cavitation-refilling on the same stem with two different solutions: 0.1 M KCl and 0.01 M $CaCl_2$. The clean water system below could repeatedly restore maximum conductivity (K_{max}) to 99.4±0.6% of the first K_{max}.

An ultrapure water system, model GYJ1-10L-S (Huachuang Inc., Chongqing, China) was used which, according to specifications, produces water with less than one particle per ml of >10 nm diameter. Before flushing, freshly filtered water was produced each morning and reagent grade KCl or $CaCl_2$ was added, and stored in a stainless steel captive air tank (CAT) model 3400-002 (SHURflo Inc., Cypress, CA). The rubber bag inside the captive air tank was about 1.5 mm thick and comprised 90 % of the surface area in contact with the salt solution. The lid and outlet

tubing was stainless steel. Contrary to popular belief, stainless steel is not rust free; rust is easily observable in the rubber bag but it does not adhere to the stainless steel surfaces. We recommend cleaning the tank twice per week to eliminate plugging-rust-particles gradually formed in the CAT. The SHURflo CAT was selected because it could be disassembled by removing 6 retaining bolts on the lid allowing removal of the rubber bag and access to the stainless steel parts normally in contact with the salt solutions. All plastic and rubber tubing of the apparatus was cleaned with bleach to kill micro-organisms followed by flushing twice with purified water. Also, the solution in the tank was left unpressurized when not in use because air slowly permeates across the rubber bag. We observed that leaving the tank pressurized for 24 h made the water weakly effervescent which could cause bubble formation in stem segments during a flush.

Cavitron measurements

The measurements on hydraulic conductivity (K_h) and vulnerability curves (VCs) were carried out using a custom rotor designed by Cochard et al. (2005) based on the centrifuge technique (Alder et al., 1997). Design details were described in detail in Cai and Tyree (2010).

Briefly, this technique makes it possible to measure the K_h while the stem segment is spinning at any given tension. A 27.4 cm segment is placed in the rotor mounted on the centrifuge. Both ends of the segment are placed in cuvettes filled with liquid (0.1 M KCl or 0.01 M $CaCl_2$) that could be replenished while spinning. A pressure difference generated by the different liquid levels of the cuvettes drives the liquid through the segment. Then the rate of movement of the liquid in the stem could be measured directly by a continuous calculation of the volume change in the cuvettes within a certain time interval.

Prior to measurements, the stems were flushed with 0.1 M KCl or 0.01 M $CaCl_2$ at 40 PSI (276 kPa) for 30 min to eliminate any native embolism. The length of time required to ensure all conduits were refilled by the flush was determined in preliminary experiments as outlined in the section “refilling and repeated cavitation cycles”. The rotor was rotated initially at 1000 RPM (0.088 MPa) without a stem segment and the thermostat set a few ^{o}C below ambient room temperature in order to have improved temperature control during measurement. Once all conduits were refilled, K_{max} was measured at 1000 RPM (0.088 MPa) in the cavitron after a stabilization time of 15 min. The tension caused by 1000 RPM was too small to cause any embolism. Subsequently a VC was obtained through stepwise increases in the spin rate of the centrifuge, subjecting the solution in the conduits to increasingly negative xylem pressures (tension = minus pressure). The K_h was collected after a 2 min stabilizing time at each 200 RPM increase. The percentage loss of hydraulic conductivity (PLC), which was attributed to embolized conduits, was computed from:

$$PLC = 100(1 - K_h/K_{max}) \qquad \text{Eq. 1}$$

The spin rate was increased until K_h was reduced to a point where the PLC ≥ 90 %.

Vulnerability curves with ≥ 9 points was deemed sufficient to characterize simple s-shaped Weibull curves. But 16 to 27 points are necessary to characterize a dual-Weibull curve. Vulnerability curves, plots of PLC versus tension (T), were fitted to a single Weibull curve Eq. 2A or a dual Weibull curve Eq. 2B through CavAnal software written by M.T.Tyree (Cai et al., 2014):

$$PLC/100 = 1 - exp[-(T/B)^{C}] \quad \text{Eq. 2A}$$

$$PLC/100 = \alpha(1 - exp[-(T/B_1)^{C_1}]) + (1-\alpha)(1 - exp[-(T/B_2)^{C_2}]) \quad \text{Eq. 2B}$$

where the constants were calculated by minimizing root mean square error (RMS_{error}).

Computation of cavitation-fatigue

Between any two cycles of cavitation and flushing of the same stem, cavitation-fatigue was computed based on absolute shift of T_x (defined above, x = 10, 20 … 90 PLC) from $T_{x,i}$ to $T_{x,j}$, where i, j were the i^{th} and j^{th} VC ($j>i$). So for absolute cavitation-fatigue (aCF_x) we computed $aCF_x = (T_{x,i} - T_{x,j})$ and for relative cavitation-fatigue (rCF_x) we computed $rCF_x = (1-T_{x,j}/T_{x,i})$. The means and standard error (SE) of each fatigue value was computed for all the stems in two different ways. The first was the difference of the means (Eq. 3A) of N values and the second was the mean of the differences (Eq. 3B) for N values. The two value of $\overline{aCF_x}$ are identical but in the test of significance in the former we are asking if the means are significantly different whereas in the latter we are asking if the difference is significantly different from zero, which was statistically more certain (see results) because the phenotypic difference between individual stems is eliminated by computing the mean of the different rather than the difference of the mean.

$$\overline{aCF_x} = \frac{1}{N}\left(\sum_{k=1}^{N} T_{x,i} - \sum_{k=1}^{N} T_{x,j}\right) \quad \text{Eq. 3A}$$

$$\overline{aCF_x} = \frac{1}{N}\sum_{k=1}^{N}\left(T_{x,i} - T_{x,j}\right) \quad \text{Eq. 3B}$$

The mean relative cavitation-fatigue (rCF_x) was computed from

$$\overline{rCF_x} = \frac{1}{N}\left(\sum_{i=1}^{N}(1 - T_{x,j}/T_{x,i})\right) \quad \text{Eq. 3C}$$

These computations allowed us to compute the fatigue shifts for up to 4 cycles of cavitation and flushing. Positive values of aCF_x and rCF_x measured loss in cavitation resistance and negative values were interpreted as an increase in cavitation resistance.

Temperature calibration

Temperature control during VC measurement is important because K_h changes 2.4% $^oC^{-1}$ as stem temperature changes because of the effect of temperature on the viscosity of water. The Beckman-Coulter centrifuge has a temperature sensor and thermostatic temperature control, but the factory sensor is mounted too near the refrigeration coils hence large temperature differences were often observed between the factory sensor and the sensor we installed near the rotor. The temperature gradient was explained by the heat generated by the spinning rotor-motor (Wang et al., 2014b). In order to correct for temperature gradients, a custom temperature sensor based on a LM335 sensor chip was installed near the rotor midway between the refrigerated wall and rotor. The temperature of the thermostat had to be adjusted down in temperature in order to achieve constant temperature in the rotor as rotor RPM increased. Experiments were done to test the adequacy of temperature control of the stem to within ±1 ^oC.

Additional experiments were done to ensure we could stabilize temperature of the stems within reasonable limits. Hydraulic conductivity was measured at constant RPM while changing the thermostat temperature setting, which caused a corresponding rapid change in stem temperature as confirmed by changes in K_h. The air temperature was logged every 10 s by our independent sensor while periodically measuring K_h at constant RPM. The stem K_h acts like a *defacto* thermometer because K_h changes in proportion to 1/viscosity of water. Preliminary experiments were performed to 'calibrate' running mean values of air temperature to the 'stem' thermometer. We found out that a 20 min running mean of air temperature correlated satisfactorily with the change in K_h when air temperature was changing rapidly (Fig. 8). Even when the thermostatic temperature was set to a constant value the instantaneous air temperature changed ±2 ^oC as the refrigeration system turned on and off, but the 20 min running mean changed less (±0.5 to 1 ^oC) when the refrigeration turned on and off more than once per 5 minutes.

Re-filling and repeated cavitation cycles (How long is enough for flushing?)

Preliminary experiments were done to determine the length of time required to refill the embolized conduits flushed at 276 kPa (40 PSI). The original conductivity (K_n) of each branch prior to flushing was measured at 1000 RPM (0.088 MPa) in the cavitron. The stem was then subjected to alternating 5 min cycles of flushing and conductivity measurements until the conductivity stabilized (did not change for three consecutive cycles of flushing). Following this, the vulnerability curve of the stem was measured.

This cycle of flushing to K_{max} and measurement of a VC was repeated 4 times. Thirty min of flushing was enough to achieve a stable K_h. On average K_h was returned to the same K_{max} as measured by the ratio of 100 % $K_{flushed}/K_{max}$ to within 99.4±0.6%. If K_h failed to reach $\geq$ 93 % following a cavitation/flush cycle then the data was thrown out.

Freeze-thaw cycles

The stems were directly flushed for 30 min at 276 kPa with 0.1 M KCl solution after collection. Unlike methods from other studies (Ameglio et al., 2001; Willson and Jackson, 2006; Christensen-Dalsgaard and Tyree, 2013), we froze and thawed the plant material at known tensions in the stems while spinning in a cavitron. We chose tensions of 0.08, 0.5, 1.0 and 1.5 MPa to continue the frost-fatigue test. In experimentally simulated freeze-thaw cycles, the stems were exposed to freezing approximately for 2 h at -5℃ (Fig. 9, thick line) and simultaneously to tensions (RPM) of 0.08 (1000), 0.5 (2400), 1.0 (3400) and 1.5 MPa (4100) respectively, following K_{max} measurements at 1000 RPM. Then the stems were thawed to the room temperature at the same tension. The conductivity after freeze-thaw treatment was measured. Subsequently, the same stems were removed, flushed for 30 min and a new VC was measured.

Partial versus full vulnerability curves comparison

In order to illustrate the connection between cavitation and frost-fatigue in 84K poplar, two different vulnerability curves were measured. The liquid used for flushing was 0.1 M KCl. The 1st VC after flushing was stopped at 50 % embolism, then the stem was removed and flushed again and then the VC was determined to > 95 % PLC.

Field conditions

Four phenological phases from fall to winter and into the next spring, including natural frost stage after the first freezing events of winter, budding stage, leaf-flushing stage and mature-leaf stage were selected for VCs measurements, in order to see if the trees growing outside showed a pattern of frost-fatigue like that induced in cavitron experiments. In all of these four stages, stems were used to measure VCs directly after flushing for 30 min with 0.1 M KCl solution at 276 kPa.

Statistics

All statistical analysis were done with the SPSS 18.0 statistics package for PC (SPSS Inc., Chicago, IL, USA) using the 0.05 significance level. Comparisons of more than two groups between all means were made with one-way ANOVA and the Duncan test. Student's *t*-tests were used to compare means between two groups or differences of means from zero when appropriate.

SUPPLEMENTAL DATA

Figure S1. Typical examples of "high resolution" VC curves with 9 to 27 points measured by Cochard rotor.

ACKNOWLEDGEMENTS

We thank Ruihua Pan for conduits diameter measurements, Ruiqing Wang, Yujie Wang, Lingling Zhang and Rongting Zhang for helpful assistance.

LITERATURE CITED

Alder NN, Pockman WT, Sperry JS, Nuismer S (1997) Use of centrifugal force in the study of xylem cavitation. J Exp Bot **48:** 665-674

Ameglio T, Bodet C, Lacointe A, Cochard H (2002) Winter embolism, mechanisms of xylem hydraulic conductivity recovery and springtime growth patterns in walnut and peach trees. Tree Physiol **22:** 1211-1220

Ameglio T, Cochard H, Ewers FW (2001) Stem diameter variations and cold hardiness in walnut trees. J Exp Bot **52:** 2135-2142

Cai J, Li S, Zhang H, Zhang S, Tyree MT (2014) Recalcitrant vulnerability curves: methods of analysis and the concept of fibre bridges for enhanced cavitation resistance. Plant Cell Environ **37:** 35-44

Cai J, Tyree MT (2010) The impact of vessel size on vulnerability curves: data and models for within-species variability in saplings of aspen, *Populus tremuloides* Michx. Plant Cell Environ **33:** 1059-1069

Christensen-Dalsgaard KK, Tyree MT (2013) Does freezing and dynamic flexing of frozen branches impact the cavitation resistance of *Malus domestica* and the *Populus* clone Walker? Oecologia **173:** 665-674

Christensen-Dalsgaard KK, Tyree MT (2014) Frost fatigue and spring recovery of xylem vessels in three diffuse-porous trees *in situ*. Plant Cell Environ **37:** 1074-1085

Christman MA, Sperry JS, Smith DD (2012) Rare pits, large vessels and extreme vulnerability to cavitation in a ring-porous tree species. New Phytol **193:** 713-720

Cirelli D, Jagels R, Tyree MT (2008) Toward an improved model of maple sap exudation: the location and role of osmotic barriers in sugar maple, butternut and white birch. Tree Physiol **28:** 1145-1155

Cochard H, Cruiziat P, Tyree MT (1992) Use of positive pressures to establish vulnerability curves - further support for the air-seeding hypothesis and implications for pressure-volume analysis. Plant Physiol **100:** 205-209

Cochard H, Damour G, Bodet C, Tharwat I, Poirier M, Ameglio T (2005) Evaluation of a new centrifuge technique for rapid generation of xylem vulnerability curves. Physiologia Plantarum **124:** 410-418

Cosgrove DJ (1997) Relaxation in a high-stress envirsnment: the molecular bases of extensible cell walls and cell enlargement. The Plant Cell **9:** 1031-1041

Cox RM, Zhu XB (2003) Effects of simulated thaw on xylem cavitation, residual embolism, spring dieback and shoot growth in yellow birch. Tree Physiol **23:** 615-624

Davis SD, Sperry JS, Hacke UG (1999) The relationship between xylem conduit diameter and cavitation caused by freezing. American Journal of Botany **86:** 1367-1372

Feng LR, Song LZ, Lin XF (2010) Research development of cold hardiness in *Populus* breeding. Ecology Evolution and Systematics **4:** 97-115

Fichot R, Brignolas F, Cochard H, Ceulemans R (2014) Vulnerability to Drought-Induced Cavitation in Poplars: Synthesis and Future Opportunities. Plant Cell Environ**:** 10.1111/pce.12491

Hacke UG, Sperry JS (2001) Functional and ecological xylem anatomy. Perspectives In Plant Ecology Evolution And Systematics **4:** 97-115

Hacke UG, Stiller V, Sperry JS, Pittermann J, McCulloh KA (2001) Cavitation fatigue. Embolism and refilling cycles can weaken the cavitation resistance of xylem. Plant Physiol **125:** 779-786

Hubbard RM, Ryan MG, Stiller V, Sperry JS (2001) Stomatal conductance and photosynthesis vary linearly with plant hydraulic conductance in ponderosa pine. Plant Cell And Environment **24:** 113-121

Jarbeau JA, Ewers FW, Davis SD (1995) The mechanism of water-stress-induced embolism in two species of chaparral shrubs. Plant Cell Environ **18:** 189-196

Johnson RW, Tyree MT, Dixon MA (1987) A requirement for sucrose in xylem sap flow from dormant maple trees. Plant Physiol **84:** 495-500

Langan SJ, Ewers FW, Davis SD (1997) Xylem dysfunction caused by water stress and freezing in two species of co-occurring chaparral shrubs. Plant Cell Environ **20:** 425-437

Mayr S, Gruber A, Bauer H (2003) Repeated freeze-thaw cycles induce embolism in drought stressed conifers (Norway spruce, stone pine). Planta **217:** 436-441

Milburn JA, O'malley PER (1984) Freeze-induced sap absorption in *Acer pseudoplatanus*: a possible mechanism. Canadian Journal of Botany **62:** 2101-2106

O'malley PER, Milburn JA (1983) Freeze-induced fluctuations in xylem sap pressure in *Acer pseudoplatanus*. Canadian Journal of Botany **61:** 3100-3106

Pittermann J, Sperry JS (2006) Analysis of freeze-thaw embolism in conifers. The interaction between cavitation pressure and tracheid size. Plant Physiol **140:** 374-382

Sperry JS, Donnelly JR, Tyree MT (1988) Seasonal occurrence of xylem embolism in sugar maple (*Acer Saccharum*). Botanical Society of America **75:** 1212-1218

Sperry JS, Saliendra NZ, Pockman WT, Cochard H, Cruiziat P, Davis SD, Ewers FW, Tyree MT (1996) New evidence for large negative xylem pressures and their measurement by the pressure chamber method. Plant Cell Environ **19:** 427-436

Sperry JS, Sullivan JE (1992) Xylem embolism in response to freeze-thaw cycles and water stress in ring-porous, diffuse-porous, and conifer species. Plant Physiol **100:** 605-613

Sperry JS, Tyree MT (1988) Mechanism of water stress-induced xylem embolism. Plant Physiol **88:** 581-587

Stiller V, Sperry JS (2002) Cavitation fatigue and its reversal in sunflower (*Helianthus annuus* L.). J Exp Bot **53:** 1155-1161

Tyree MT (1983) Maple sap uptake, exudation, and pressure changes correlated with freezing exotherms and thawing endotherms. Plant Physiol **73:** 277-285

Tyree MT, Davis SD, Cochard H (1994) Biophysical perspectives of xylem evolution - is there a tradeoff of hydraulic efficiency for vulnerability to dysfunction. Iawa Journal **15:** 335-360

Tyree MT, Zimmermann MH (2002) Xylem structure and the ascent of sap, Ed 2. Springer-Verlag, Berlin, Germany

van Ieperen W, van Gelder A (2006) Ion-mediated flow changes suppressed by minimal calcium presence in xylem sap in *Chrysanthemum* and *Prunus laurocerasus*. J Exp Bot **57:** 2743-2750

Wang R, Zhang L, Zhang S, Cai J, Tyree MT (2014a) Water relations of Robinia pseudoacacia L.: do vessels cavitate and refill diurnally or are R-shaped curves invalid in Robinia? Plant Cell Environ **37:** 2667-2678

Wang YJ, Burlett R, Feng F, Tyree MT (2014b) Improved precision of hydraulic conductance measurements using a Cochard rotor in two different centrifuges. Journal of Plant Hydraulics **1:** 0007e

Willson CJ, Jackson RB (2006) Xylem cavitation caused by drought and freezing stress in four co-occurring Juniperus species. Physiologia Plantarum **127:** 374-382

Yang S, Tyree MT (1992) A theoretical-model of hydraulic conductivity recovery from embolism with comparison to experimental-data on Acer Saccharum. Plant Cell Environ **15:** 633-643

Zhou YX, Fu YQ, Fan JF, Liu YY, Gao JS, Wang J, Fu J, Li JA (2007) Growth characteristics and crossability of poplar 84K. Journal of Northeast Forestry University **35:** 11-12

Figure 1. Plotted are mean vulnerability curves measured for the same stem exposed to 4 cycles of cavitation-refilling (flushing) and VCs measurements with 0.1 M KCl solution (A) and 0.01 M $CaCl_2$ solution (B). The mean and SE (N = 7 for KCl values and N = 6 for $CaCl_2$ values) of all curves were computed. See Table I for the % recovery of hydraulic conductivity after flushes.

Figure 2. This shows two quantitative measures of cavitation-fatigue for KCl flushed samples. The fatigue values were calculated from the mean of the differences Eq. 3B (see methods), and is considered a more powerful test of differences between VCs. A: Mean relative cavitation-fatigue (rCF_x) versus x = the PLC at which rCF_x was evaluated. Solid squares compare 1st to 2nd VC, y = -0.3612x + 74.012 (R^2 = 0.9952, p = 2E-09); solid triangles compare 2nd to 3rd VC, y = 0.2335x - 31.992 (R^2 = 0.9444, p =1E-05); solid circles compare 3rd to 4th VC, y = 0.1436x - 16.341 (R^2 = 0.95, p =8E-06); and solid diamonds compare 2nd to 4th VC, y = 0.43x - 52.274 (R^2 = 0.9489, p =9E-06). B: Mean change in absolute cavitation-fatigue (aCF_x) versus x = the PLC at which aCF_x was evaluated. Hollow squares compare 1st to 2nd VC, y = -7E-05x^2 + 0.0086x + 0.9352 (R^2 = 0.9758, p =1E-5), however, the individual points were not different from each other significantly (p =0.334); hollow triangles compare 2nd to 3rd VC, y = -0.0006x - 0.1146 (R^2 = 0.7535, p =0.0024); hollow circles compare 3rd to 4th VC, y = 0.0004x - 0.099 (R^2 = 0.5669, p =0.019); and hollow diamonds compare 2nd to 4th VC, y = 3E-05x^2 - 0.0029x - 0.1636 (R^2 = 0.9877, p =2E-6). Error bars are SE. Symbols marked without '*' marks were not significantly different from zero. The p-values in the linear regressions give the probability that the slope is zero.

Figure 3. This shows two quantitative measures of cavitation-fatigue for $CaCl_2$ flushed samples. The fatigue values were calculated from the mean of the differences Eq. 3B (see methods), and is considered a more powerful test of differences between VCs. A: Mean relative cavitation-fatigue (rCF_x) versus x = the PLC at which rCF_x was evaluated. Solid squares compare 1st to 2nd VC, y = -0.3333x + 68.857 (R^2 = 0.9961, p = 1E-09); solid triangles compare 2nd to 3rd VC, y = -0.0018x + 0.1707 (R^2 = 0.9233, p = 4E-05); and solid circles compare 3rd to 4th VC, y = 0.3293x - 42.064 (R^2 = 0.9413, p = 1E-05). B: Mean change in absolute cavitation-fatigue (aCF_x) versus x = the PLC at which aCF_x was evaluated. Hollow squares compare 1st to 2nd VC, y = -6E-05x^2 + 0.0078x + 0.8899 (R^2 = 0.9661, p = 4E-05), however, the individuals were not different from each other significantly (p = 0.408); hollow triangles compare 2nd to 3rd VC, y = -0.0005x + 0.1225 (R^2 = 0.58, p = 0.017); hollow circles compare 3rd to 4th VC, y = -0.0009x - 0.1599 (R^2 = 0.8087, p = 0.001). Error bars are SE. Symbols with no '*' marks were not significantly different from zero. The p-values in the linear regressions give the probability that the slope is zero.

627 Figure 4. Vulnerability curves measured in stems following a freeze-thaw cycle (f-t) at varying
628 tension. Frost induced embolism was removed by flushing before measuring the above VCs,
629 hence the double s-curves were caused by frost-fatigue. The mean of 6~8 VCs were measured on
630 flushed stems by the cavitron technique where each curve was fitted with a dual Weibull, then the
631 mean and SE of all 6~8 best-fit curves were computed.
632
633 Figure 5. The squares show the impact of freezing on changes of K_h expressed as % of K_{max} before
634 freezing. Error bars are ± SE (N = 6 to 8). The y-axis can also be interpreted as 100% - the PLC
635 induced by freezing + the tension on the x-axis. The solid line is a Weibull equation fit of the
636 squares. The dashed line shows the mean impact of tension alone, without freezing, on %
637 maximum K_h; these values were re-plotted from the 1st VC in Fig. 1A (100% - PLC induced by
638 tension alone). The double arrow can be interpreted as the amount of tension added by the
639 freezing or thawing of tissue.
640
641 Figure 6. Vulnerability curves measured before and after 50 % embolism induced in stems. The
642 mean and SE of all 6 best-fit curves before (solid curve) and after (dashed curve) 50% embolism
643 was induced by a tension of about 2.25 MPa; the stems were flushed between the first and second
644 curve. The dashed curve was fitted with a dual Weibull, which is the sum of two s-shaped Weibull
645 curves.
646
647 Figure 7. A: Vulnerability curves measured when stems were in four phenological phases, natural
648 frost stage, budding stage, leaf-flush stage and mature-leaf stage. VCs measurements in the
649 natural frost stage were based on N = 12 samples. VCs measurements in the budding stage and
650 leaf-flush stage were based on N = 6 samples respectively. The mature-leaf stage were based on N
651 = 7 samples. The mean of these VCs measured on flushed stems by the cavitron technique where
652 each curve was fitted with a dual Weibull, then the mean and SE were computed from the
653 individual Weibull curves. The dual Weibull fit is the sum of two Weibull curves, the first s-
654 shaped Weibull of each phonological phases are plotted to their theoretical plateaus for clarity and
655 the plateau values on the y-axis = α in Eq. 2B. B: Shows a plot of minimum and maximum air
656 temperatures recorded by a weather station 4 km of the location of the sampled trees.
657
658 Figure 8. A: This shows the tempo of change in air temperature and the 20 min running mean of
659 air temperature measured 2 cm from the rotor during the experiment shown in B. B: Shows the K_h
660 in stem versus the 20 min running mean of air temperature (RmTC20). The regression of K_h
661 versus RmTC20 was y = 0.0648x + 1.8474, R^2 = 0.9826, $p \leq 10^{-23}$, and the close correlation

means that the 20 min running mean air temperature was an acceptable predictor of stem temperature. However the dependence of K_h on stem temperature was a less (lower slope) then predicted from 1/viscosity of water in an ideal pipe (TheorStem), which had a regression of y = 0.0774x + 1.8472, $R^2 = 0.9994$, $p \leq 10^{-23}$.

Figure 9. This shows a typical plot of temperature versus time for a typical freeze-thaw cycle. Air temperature (thin line) in the cavitron was collected every 10s. However, 20 min running mean of air temperature (thick line) reflected more precisely the correct stem temperature (see Fig. 8). The stems thawed more slowly than they froze because the centrifuge did not have active heating; hence the stems and centrifuge was passively heated by the warm lab.

Figure S1. Typical examples of "high resolution" VC curves with 9 to 27 points measured by Cochard rotor. A: Typical examples of VC curves with 9 to 13 points measured in cavitation-fatigue experiments. B: Typical examples of VC curves with 24 to 25 points measured after freeze-thaw treatment.

Table I. Percentage restoration of conductivity (K_{h_i}) after flushing followed by VCs measurement using 0.1 M KCl and 0.01 M $CaCl_2$ solution, respectively. Letter *i* represents the i^{th} flush followed by the i^{th} VC measurement (i = 1, 2, 3, 4). The data are based on means ± SE of 7 samples (KCl) and 6 samples ($CaCl_2$). Also shown is percentage recovery of K_h after a freeze/thaw event in stems flushed with KCl at different freeze-thaw tensions (F-T Tension); shown are mean ± SE of N = 6 to 8. $K_{f\text{-}t}$ = K_h recovered by flushing after the freeze-thaw event and K_{max} = K_h of flushed stems before freezing.

Solution	K_{h_2}/K_{h_1}	K_{h_3}/K_{h_1}		K_{h_4}/K_{h_1}
KCl	100.2±1.7%	100.2±0.9%		95.4±1.1%
$CaCl_2$	98.0±1.3%	103.1±1.9%		100.0±1.4%
F-T Tension (MPa)	0.088	0.50	1.0	1.5
$K_{f\text{-}t}/K_{max}$	100.85±1.58%	98.68±2.01%	97.11±2.09%	95.40±1.50%

Table II. Statistical analysis of VCs measured in the same stem undergoing 4 cycles of cavitation-refilling and VCs measurements with 0.1 M KCl and 0.01 M $CaCl_2$ solutions respectively. Significance tests focus on the impact of salts (KCl vs $CaCl_2$) used for the flush. T_x represents the tension at which certain percentage loss of conductivity was caused (10, 20 … 90 %). The values are means ± SE of 7 samples using 0.1 M KCl solution and 6 samples using 0.01 M $CaCl_2$ solution. Significance levels (testing the impact of solution at any PLC): '*' means $p < 0.05$.

PLC	1st VC		2nd VC		3rd VC			4th VC	
(%)	T_x(KCl)	T_x($CaCl_2$)	T_x(KCl)	T_x($CaCl_2$)	T_x(KCl)	T_x($CaCl_2$)		T_x(KCl)	T_x($CaCl_2$)
10	1.38±0.1	1.41±0.1	0.38±0.0	0.46±0.0	0.48±0.0	0.35±0.0	*	0.56±0.0	0.50±0.0
20	1.64±0.1	1.66±0.1	0.54±0.0	0.63±0.0	0.67±0.0	0.52±0.0	*	0.75±0.0	0.69±0.0
30	1.82±0.1	1.84±0.0	0.68±0.0	0.77±0.0	0.81±0.0	0.66±0.0	*	0.90±0.0	0.86±0.0
40	1.98±0.0	2.00±0.0	0.81±0.0	0.90±0.1	0.95±0.0	0.79±0.0	*	1.04±0.0	1.00±0.0
50	2.12±0.0	2.14±0.0	0.93±0.0	1.03±0.1	1.08±0.0	0.92±0.0	*	1.17±0.0	1.13±0.0
60	2.27±0.0	2.28±0.0	1.07±0.1	1.16±0.1	1.22±0.0	1.06±0.0		1.31±0.0	1.28±0.0
70	2.42±0.0	2.43±0.0	1.22±0.1	1.31±0.1	1.38±0.0	1.21±0.0		1.45±0.0	1.44±0.1
80	2.59±0.0	2.60±0.0	1.40±0.1	1.49±0.1	1.56±0.0	1.41±0.1		1.63±0.0	1.63±0.1
90	2.83±0.0	2.82±0.0	1.67±0.1	1.74±0.1	1.82±0.1	1.68±0.1		1.87±0.0	1.91±0.1

Table III. Significance analysis results are shown for VCs quantified in Table II. The significance tests focused on the differences between VC curve numbers: 1, 2, 3, or 4 based on the means in Table II for VCs measurements with 0.1 M KCl solution (left) or 0.01 M $CaCl_2$ solution (right). T_x represents the tension at which certain percentage loss of conductivity was caused (10, 20 ... 90 %). Letters *i* and *j* indicate the i^{th} VC after the i^{th} flushing and the j^{th} VC after the j^{th} flushing, respectively. The significance analysis of VCs with KCl solution was based on N = 7 samples. The $CaCl_2$ solution VCs were based on N = 6 samples. Significance levels (testing the impact of solution at any PLC): '*' means $p < 0.05$.

i^{th} VC vs j^{th} VC	T_x (KCl)									T_x ($CaCl_2$)								
	10	20	30	40	50	60	70	80	90	10	20	30	40	50	60	70	80	90
1st vs 2nd	*	*	*	*	*	*	*	*	*	*	*	*	*	*	*	*	*	*
1st vs 3rd	*	*	*	*	*	*	*	*	*	*	*	*	*	*	*	*	*	*
1st vs 4th	*	*	*	*	*	*	*	*	*	*	*	*	*	*	*	*	*	*
2nd vs 3rd																		
2nd vs 4th		*	*	*	*	*	*											
3rd vs 4th																		

Table IV. Significance analysis of tensions at any given PLC in vulnerability curves of four phenological phases in stems collected from trees growing outdoors. T_x represents the tension at which certain percentage loss of conductivity was caused (10, 20 ... 90 %). Data are based on means ± SE. The same small letters indicate the significant difference $p > 0.05$

T_x	Phenological Phase			
	Natural frost	budding	Leaf-flushing	Mature-leaf
T_{10}	0.84±0.12a	0.65±0.07a	1.06±0.26a	0.96±0.15a
T_{20}	1.47±0.14a	1.17±0.19a	1.52±0.23a	1.56±0.11a
T_{30}	1.80±0.11a	1.55±0.21a	1.87±0.12a	1.79±0.09a
T_{40}	2.05±0.08a	1.96±0.12a	2.07±0.07a	1.95±0.07a
T_{50}	2.23±0.07a	2.22±0.06a	2.23±0.05a	2.08±0.05a
T_{60}	2.39±0.06a	2.41±0.05a	2.36±0.05ab	2.20±0.05b
T_{70}	2.53±0.06a	2.59±0.04a	2.49±0.06a	2.31±0.04b
T_{80}	2.71±0.07a	2.77±0.03a	2.63±0.08a	2.44±0.05b
T_{90}	2.95±0.07a	3.01±0.05a	2.80±0.10ab	2.61±0.06b

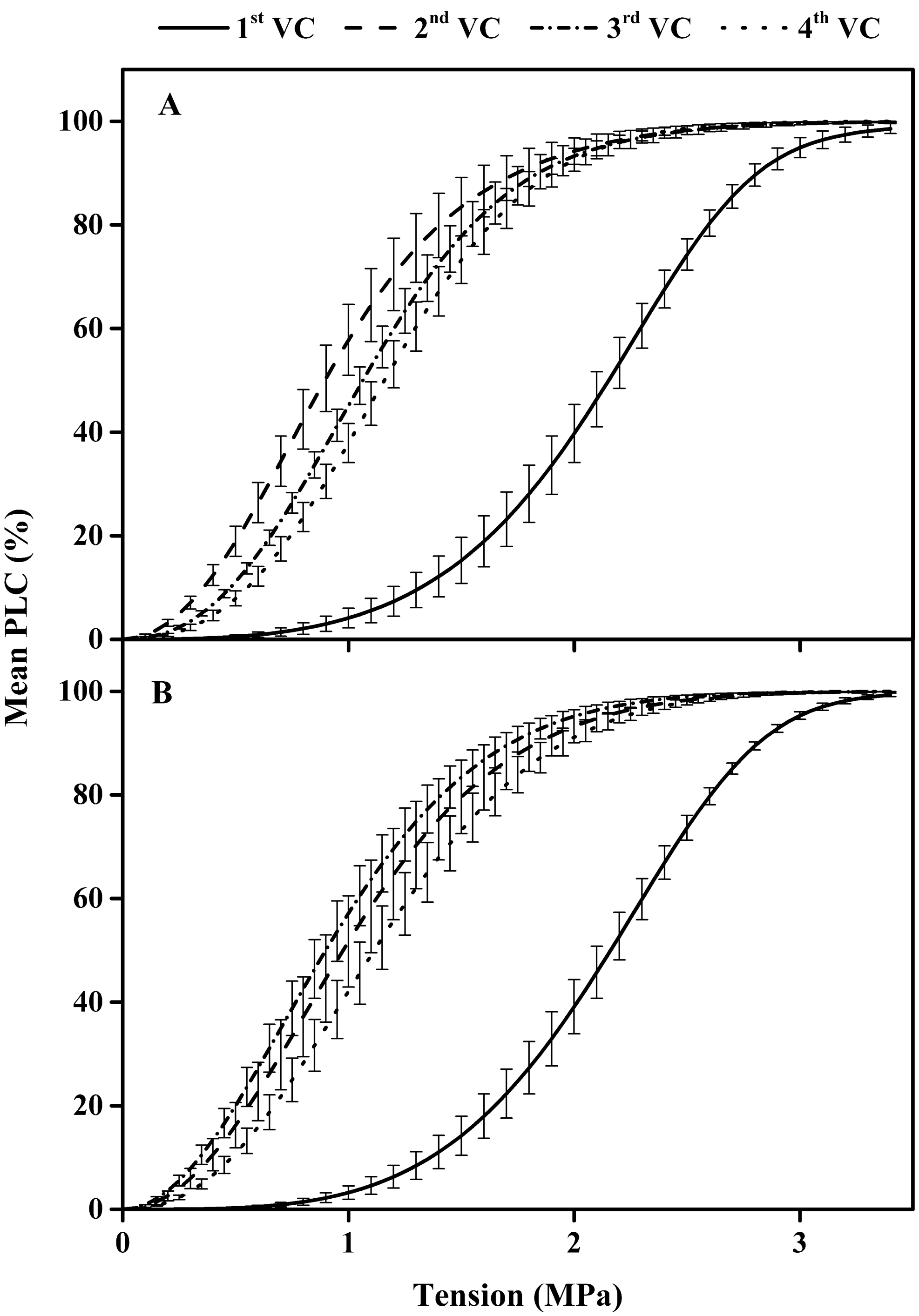

Figure 1. Plotted are mean vulnerability curves measured for the same stem exposed to 4 cycles of cavitation-refilling (flushing) and VCs measurements with 0.1 M KCl solution (A) and 0.01 M $CaCl_2$ solution (B). The mean and SE (N = 7 for KCl values and N = 6 for $CaCl_2$ values) of all curves were computed. See Table I for the % recovery of hydraulic conductivity after flushes.

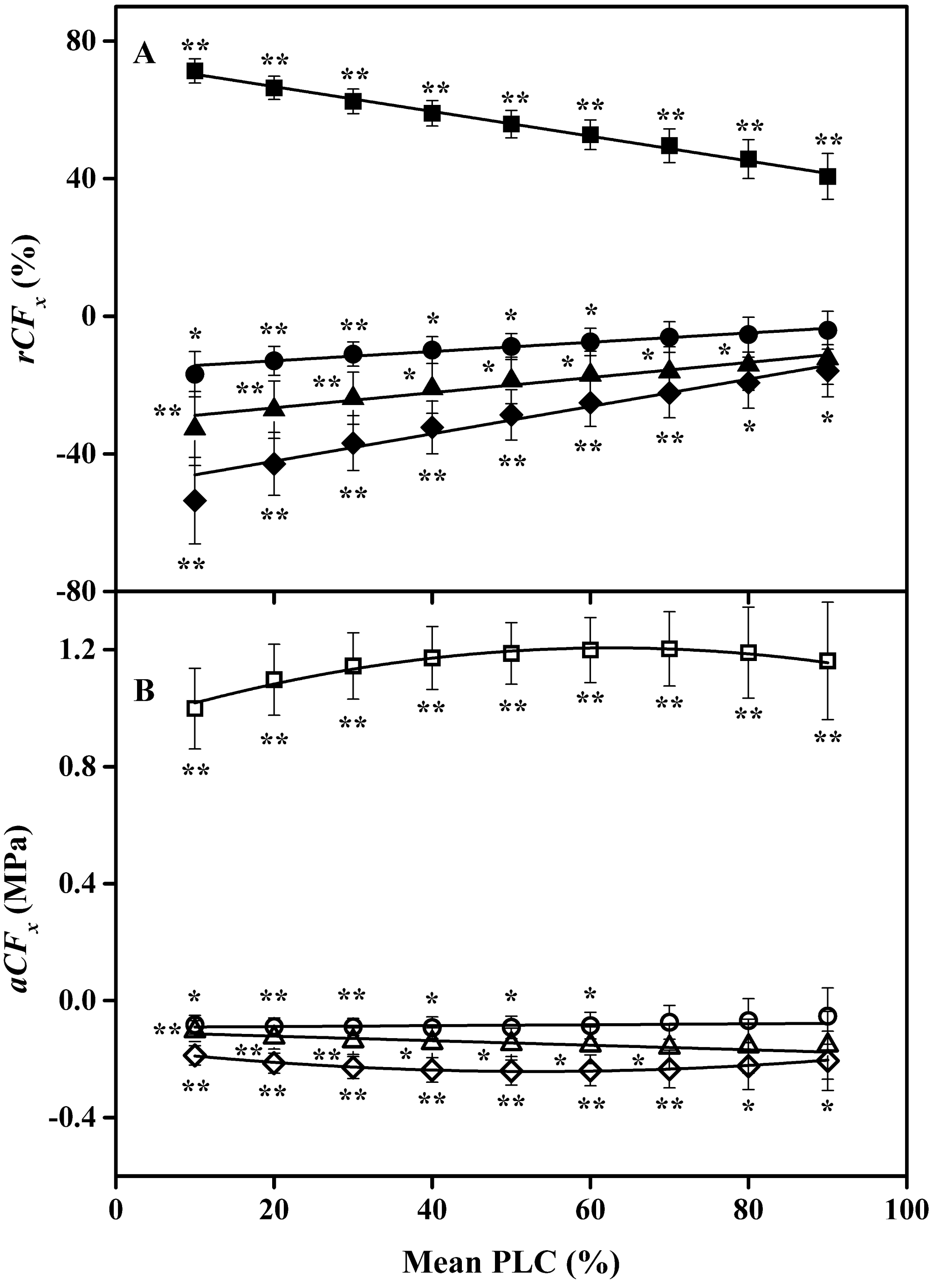

Figure 2. This shows two quantitative measures of cavitation-fatigue for KCl flushed samples. The fatigue values were calculated from the mean of the differences Eq. 3B (see methods), and is considered a more powerful test of differences between VCs. A: Mean relative cavitation-fatigue (rCF_x) versus x = the PLC at which rCF_x was evaluated. Solid squares compare 1st to 2nd VC, y = -0.3612x + 74.012 (R^2 = 0.9952, p =2E-09); solid triangles compare 2nd to 3rd VC, y = 0.2335x - 31.992 (R^2 = 0.9444, p = 1E-05); solid circles compare 3rd to 4th VC, y = 0.1436x - 16.341 (R^2 = 0.95, p = 8E-06); and solid diamonds compare 2nd to 4th VC, y = 0.43x - 52.274 (R^2 = 0.9489, p = 9E-06). B: Mean change in absolute cavitation-fatigue (aCF_x) verus x = the PLC at which aCF_x was evaluated. Hollow squares compare 1st to 2nd VC, y = -7E-05x^2 + 0.0086x + 0.9352 (R^2 = 0.9758, p =1E-5), however, the individual points were not different from each other significantly (p = 0.334); hollow triangles compare 2nd to 3rd VC, y = -0.0006x - 0.1146 (R^2 = 0.7535, p =0.0024); hollow circles compare 3rd to 4th VC, y = 0.0004x - 0.099 (R^2 = 0.5669, p = 0.019); and hollow diamonds compare 2nd to 4th VC, y = 3E-05x^2 - 0.0029x - 0.1636 (R^2 = 0.9877, p = 2E-6). Error bars are SE. Symbols marked without '*' marks were not significantly different from zero. The p-values in the linear regressions give the probability that the slope is zero.

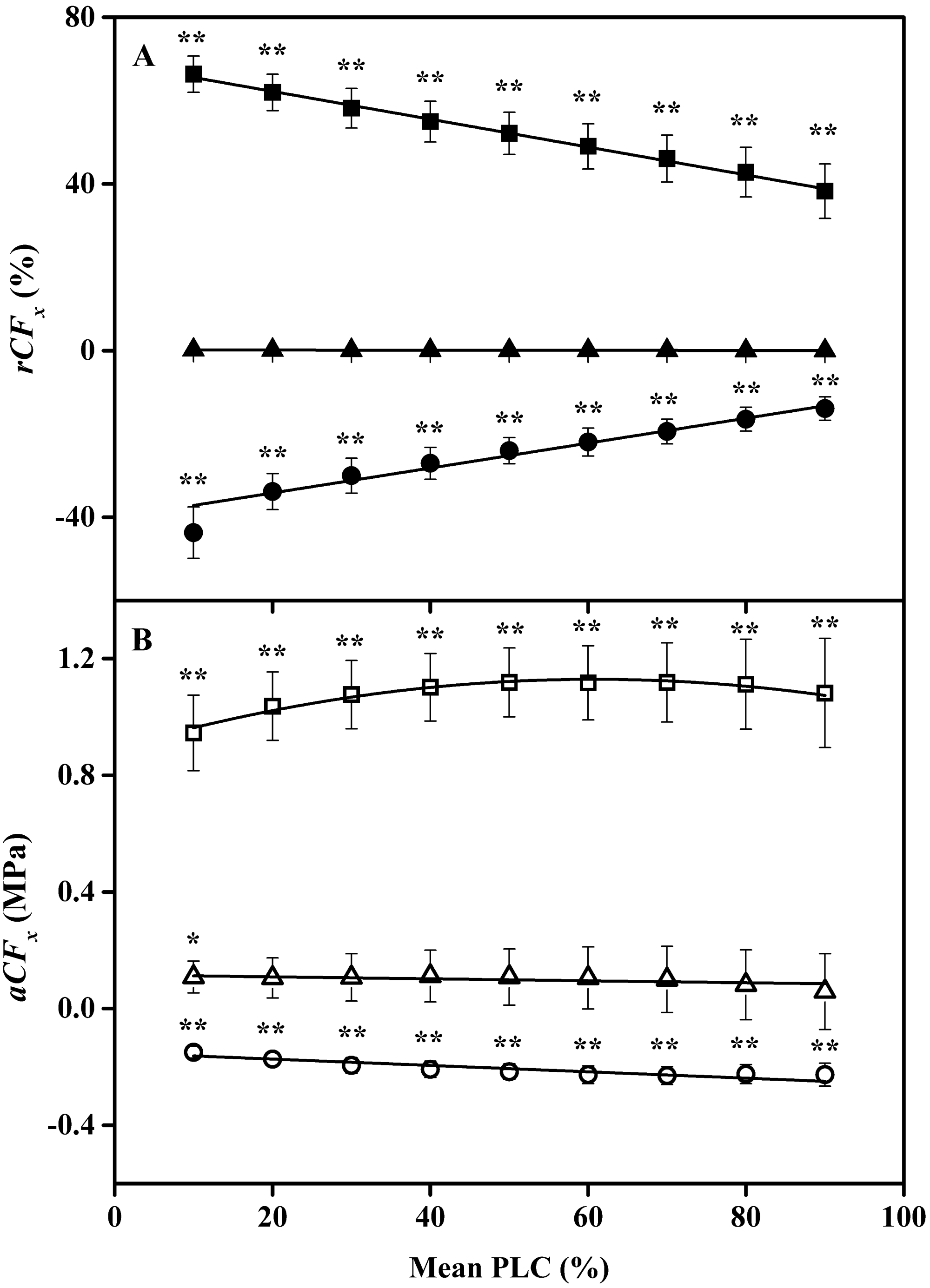

Figure 3. This shows two quantitative measures of cavitation-fatigue for $CaCl_2$ flushed samples. The fatigue values were calculated from the mean of the differences Eq. 3B (see methods), and is considered a more powerful test of differences between VCs. A: Mean relative cavitation-fatigue (rCF_x) versus x = the PLC at which rCF_x was evaluated. Solid squares compare 1st to 2nd VC, $y = -0.3333x + 68.857$ ($R^2 = 0.9961$, p =1E-09); solid triangles compare 2nd to 3rd VC, $y = -0.0018x + 0.1707$ ($R^2 = 0.9233$, p=4E-05); and solid circles compare 3rd to 4th VC, $y = 0.3293x - 42.064$ ($R^2 = 0.9413$, p = 1E-05). B: Mean change in absolute cavitation-fatigue (aCF_x) verus x = the PLC at which aCF_x was evaluated. Hollow squares compare 1st to 2nd VC, $y = -6E\text{-}05x^2 + 0.0078x + 0.8899$ ($R^2 = 0.9661$, p = 4E-05), however, the individuals were not different from each other significantly (p = 0.408); hollow triangles compare 2nd to 3rd VC, $y = -0.0005x + 0.1225$ ($R^2 = 0.58$, p = 0.017); hollow circles compare 3rd to 4th VC, $y = -0.0009x - 0.1599$ ($R^2 = 0.8087$, p =0.001). Error bars are SE. Symbols with no '*' marks were not significantly different from zero. The p-values in the linear regressions give the probability that the slope is zero.

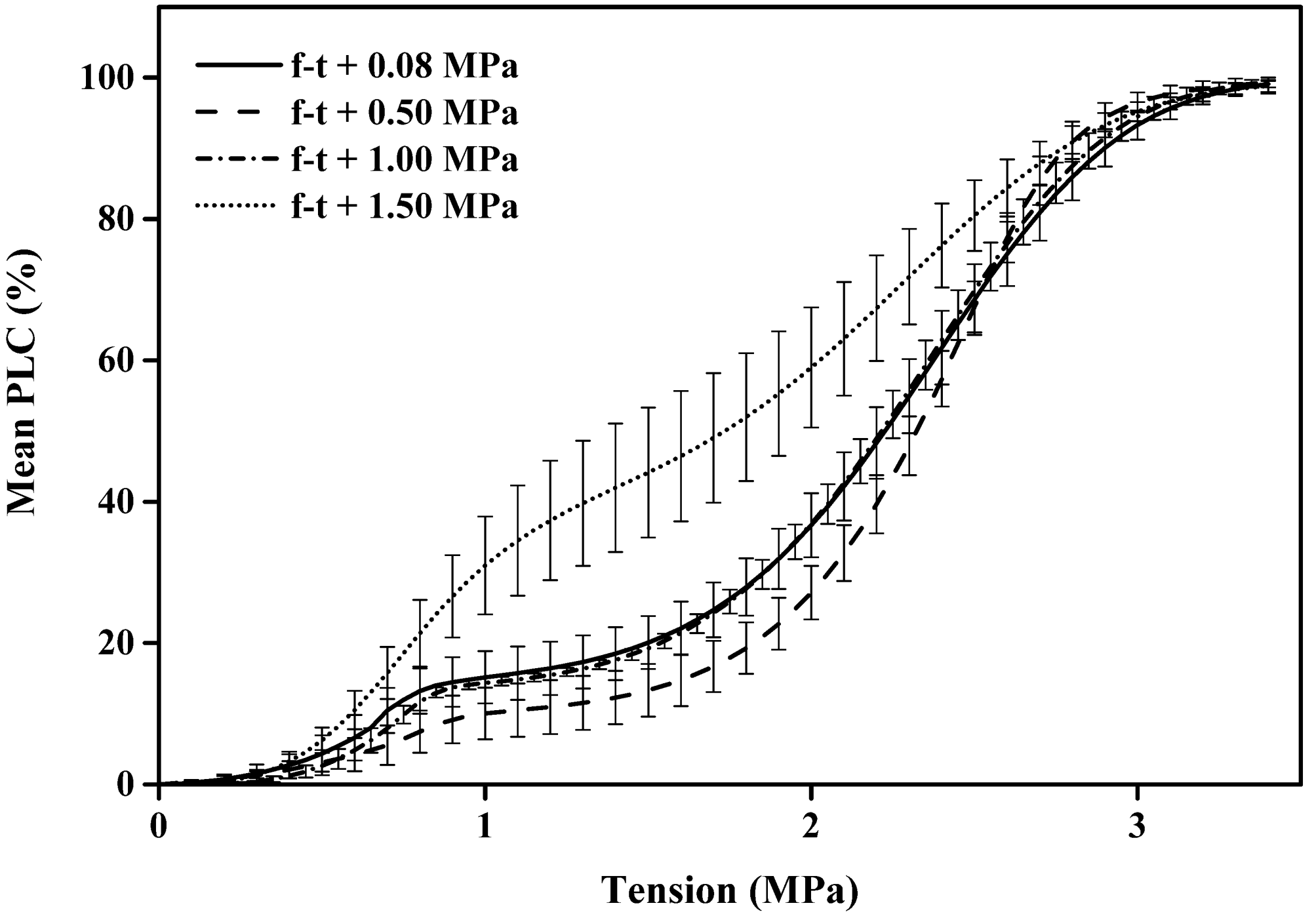

Figure 4. Vulnerability curves measured in stems following a freeze-thaw cycle (f-t) at varying tension. Frost induced embolism was removed by flushing before measuring the above VCs, hence the double s-curves were caused by frost-fatigue. The mean of 6~8 VCs were measured on flushed stems by the cavitron technique where each curve was fitted with a dual Weibull, then the mean and SE of all 6~8 best-fit curves were computed.

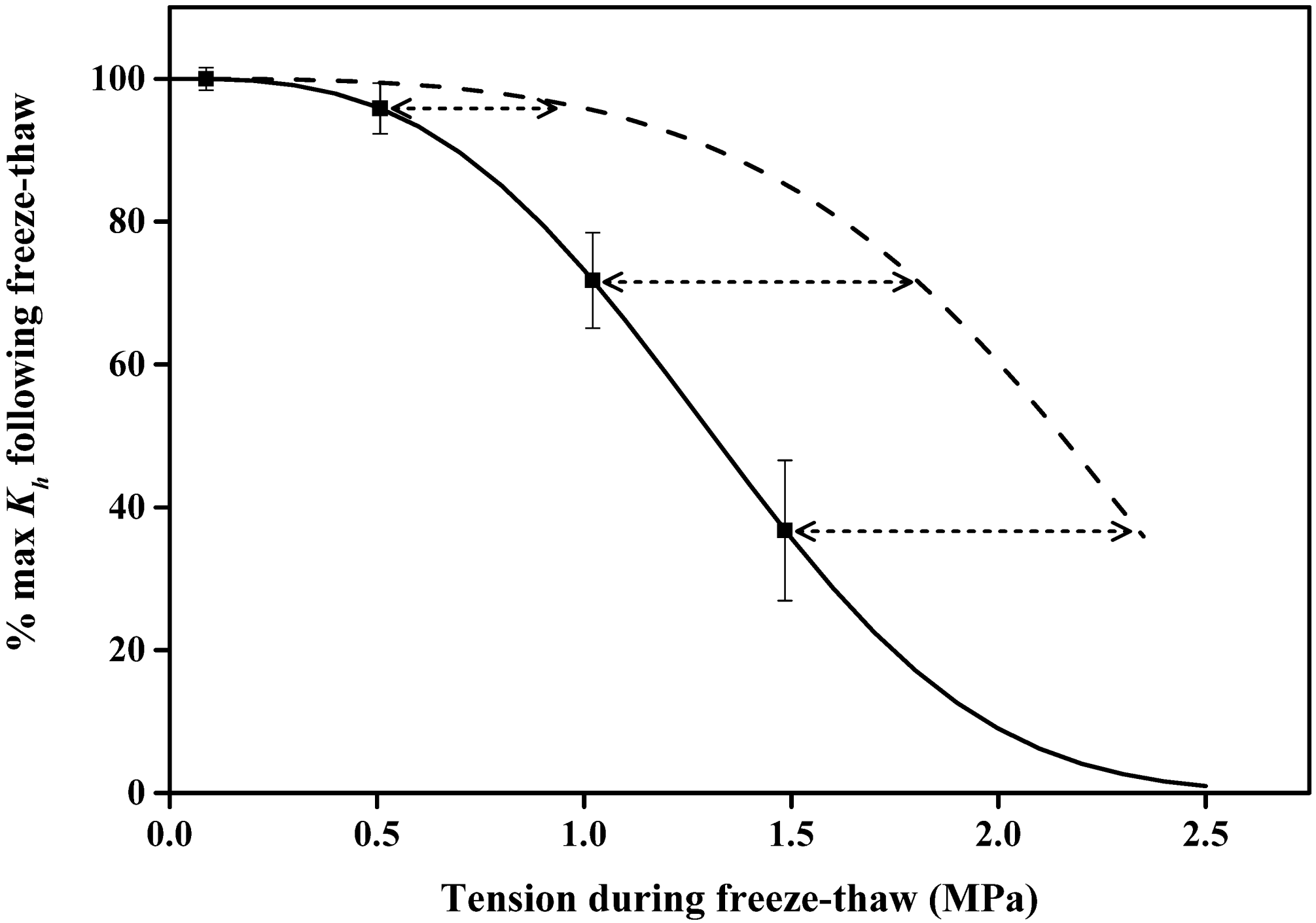

Figure 5. The squares show the impact of freezing on changes of K_h expressed as % of K_{max} before freezing. Error bars are ± SE (N = 6 to 8). The y-axis can also be interpreted as 100% - the PLC induced by freezing + the tension on the x-axis. The solid line is a Weibull equation fit of the squares. The dashed line shows the mean impact of tension alone, without freezing, on % maximum K_h; these values were re-plotted from the 1st VC in Fig. 1A (100% - PLC induced by tension alone). The double arrow can be interpreted as the amount of tension added by the freezing or thawing of tissue.

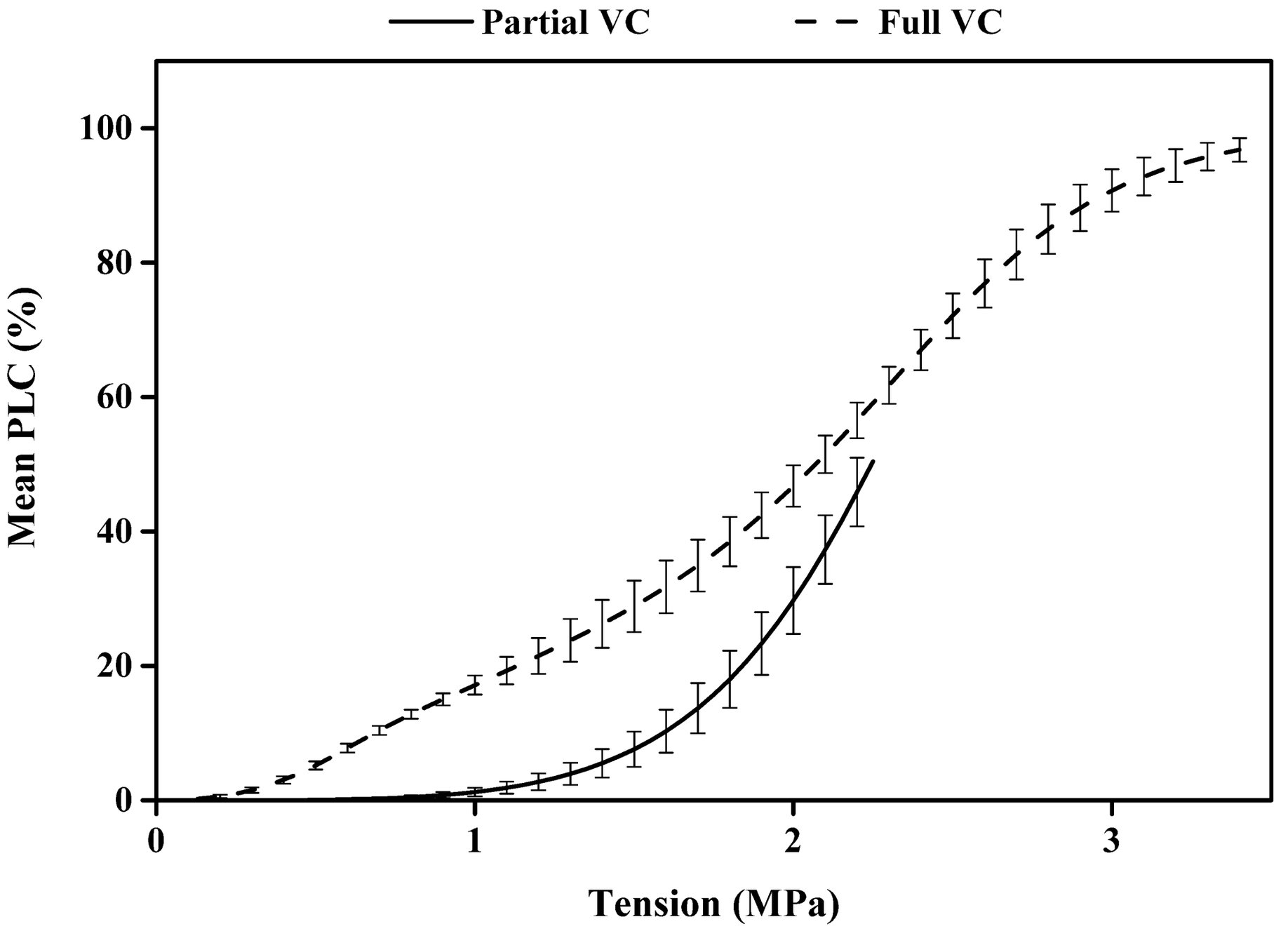

Figure 6. Vulnerability curves measured before and after 50 % embolism induced in stems. The mean and SE of all 6 best-fit curves before (solid curve) and after (dashed curve) 50 % embolism was induced by a tension of about 2.25 MPa; the stems were flushed between the first and second curve. The dashed curve was fitted with a dual Weibull, which is the sum of two s-shaped Weibull curves.

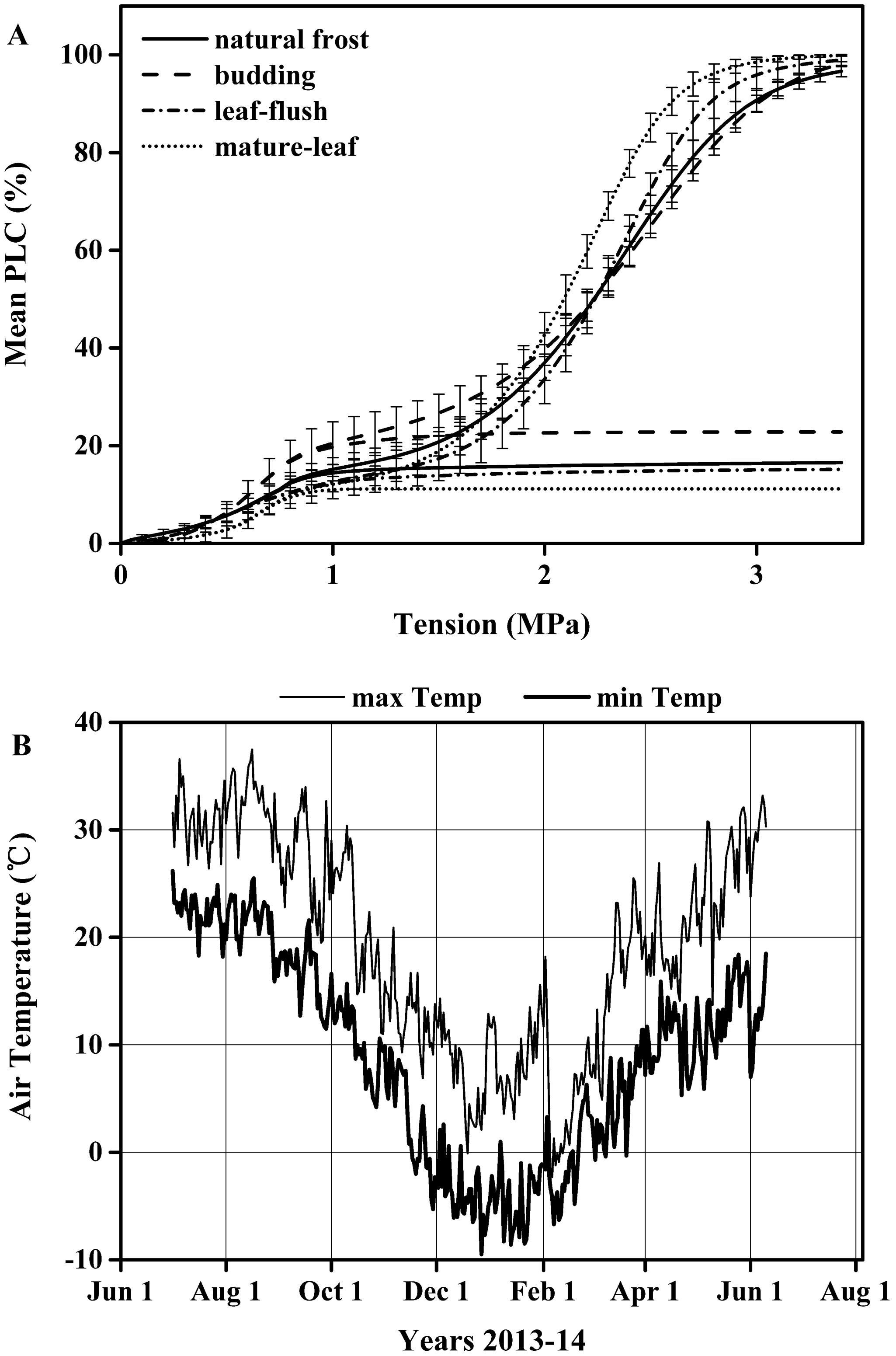

Figure 7. A: Vulnerability curves measured when stems were in four phenological phases, natural frost stage, budding stage, leaf-flush stage and mature-leaf stage. VCs measurements in the natural frost stage were based on N = 12 samples. VCs measurements in the budding stage and leaf-flush stage were based on N = 6 samples respectively. The mature-leaf stage were based on N = 7 samples. The mean of these VCs measured on flushed stems by the cavitron technique where each curve was fitted with a dual Weibull, then the mean and SE were computed from the individual Weibull curves. The dual Weibull fit is the sum of two Weibull curves, the first s-shaped Weibull of each phonological phases are plotted to their theoretical plateaus for clarity and the plateau values on the y-axis = α in Eq. 2B. B: Shows a plot of minimum and maximum air temperatures recorded with 4 km of the location of the sampled trees.

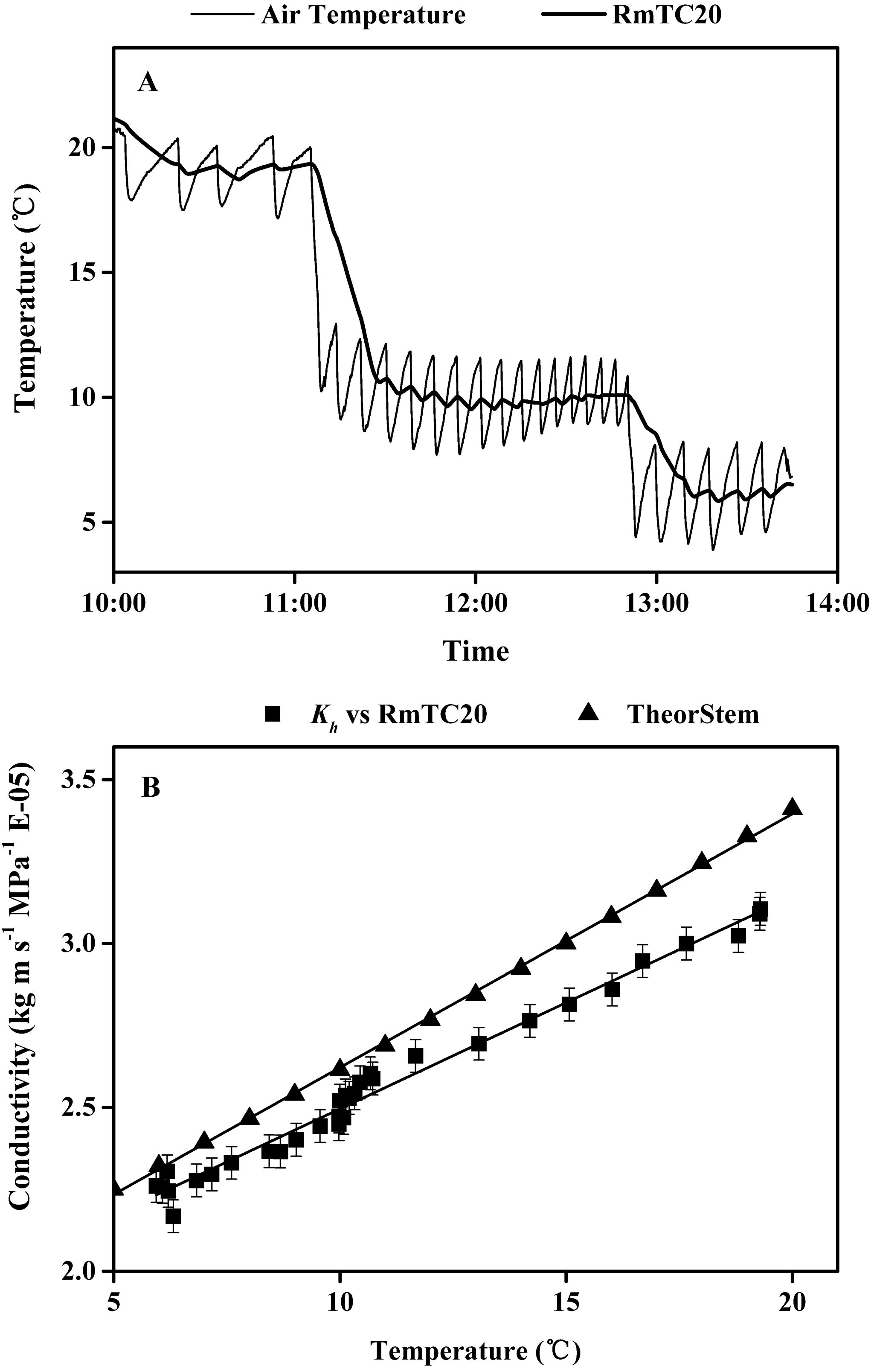

Figure 8. A: This shows the tempo of change in air temperature and the 20 min running mean of air temperature measured 2 cm from the rotor during the experiment shown in B. B: Shows the K_h in stem versus the 20 min running mean of air temperature (RmTC20). The regression of K_h versus RmTC20 was y = 0.0648x + 1.8474, $R^2 = 0.9826$, $p \leq 10^{-23}$, and the close correlation means that the 20 min running mean air temperature was an acceptable predictor of stem temperature. However the dependence of K_h on stem temperature was a less (lower slope) then predicted from 1/viscosity of water in an ideal pipe (TheorStem), which had a regression of y = 0.0774x + 1.8472, $R^2 = 0.9994$, $p \leq 10^{-23}$.

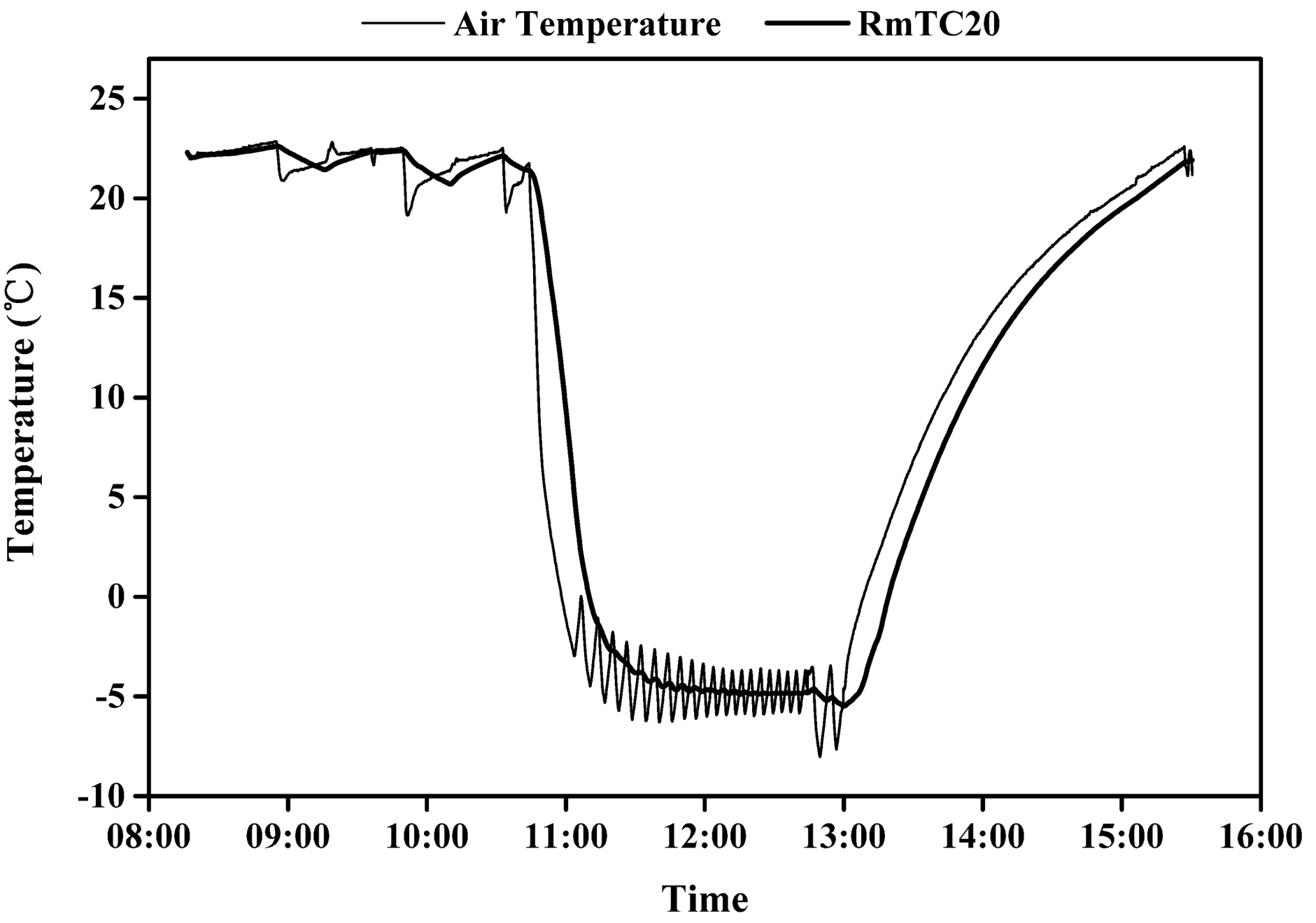

Figure 9. This shows a typical plot of temperature versus time for a typical freeze-thaw cycle. Air temperature (thin line) in the cavitron was collected every 10s. However, 20 min running mean of air temperature (thick line) reflected more precisely the correct stem temperature (see Fig. 8). The stems thawed more slowly than they froze because the centrifuge did not have active heating; hence the stems and centrifuge was passively heated by the warm lab.